13th International Conference on Applications of Statistics and Probability in Civil Engineering, ICASP13
Seoul, South Korea, May 26-30, 2019

Efficiency of Spectral Acceleration for Seismic Assessment of Offshore Wind Turbines

Ahmer Ali
Graduate Student, Dept. of Civil Engineering, University of Bristol, Bristol, United Kingdom

Raffaele De Risi
Lecturer, Dept. of Civil Engineering, University of Bristol, Bristol, United Kingdom

Katsuichiro Goda
Associate Professor, Dept. of Earth Sciences, Western University, London, Canada

Anastasios Sextos
Professor, Dept. of Civil Engineering, University of Bristol, Bristol, United Kingdom

Zhiwang Chang
Assistant Professor, Dept. of Civil Engineering, Southwest Jiaotong University, Chengdu, China

ABSTRACT: An efficient choice of intensity measure (IM) is vital for reliable estimation of structural performance. Offshore wind turbine (OWT) installations are continually planned and executed in active seismic regions, however, present understanding on their seismic vulnerability to various earthquake types and potentially suitable IMs to quantify the seismic response is yet incomprehensive. This study evaluates the efficiency of spectral acceleration S_a to describe seismic performance of OWTs for serviceability, ultimate and emergency shutdown conditions through a probabilistic regression model. In addition, sensitivity of structural reliability to pulse and non-pulse records is examined. Results emphasize the efficiency of $S_a(T_1)$ and $AvgS_a$ at serviceability, ultimate limit state and emergency shutdown, respectively, with reasonable dispersion. Regardless of pulse and non-pulse classification, 5MW is found vulnerable to crustal records with strong vertical acceleration and PGV content.

1. INTRODUCTION

Installed wind power continues to expand worldwide with American and several Asian markets, including China, Japan, Taiwan and South Korea, taking steps to develop domestic offshore industry and enhance deployment. Wind and wave-induced loads are generally considered as key design drivers for OWTs, however, in active tectonic regions such as, USA, China, Japan, India, Southern Europe, etc., periodic strong earthquakes may additionally affect the design for wind turbines which has been marginally addressed in the literature (Kim et al. 2014; Alati et al. 2015).

The consideration of earthquake loads is not quite straightforward, as it depends on the seismo-tectonic nature of the region. In near-fault crustal regions, ground motions have long been known to inherit strong velocity pulses leading to severe damages, as structures are exposed to large amount of seismic energy in a short duration (Kalkan and Kunnath 2006). De Risi et al. (2018), for the first-time studied response sensitivity of OWTs to earthquake types and observed vulnerability of 2MW monopile-supported turbine to extreme un-scaled crustal and interplate records. However, no explicit attention was paid to the effects of pulse-like ground motions.

In the context of performance-based engineering, choice of an efficient intensity measure (IM) is paramount to decouple seismic hazard and structure performance assessment. First-mode spectral acceleration $S_a(T_1)$ is the most conventionally used IM for response

prediction of structures. However, the efficiency of $S_a(T_1)$ has been vastly questioned for structures sensitive to higher-modes. Thus, various elastic, inelastic, structure-specific and non-structure specific, scalar and vector IMs have been suggested in the literature for a wide range of short and long vibration periods (Ebrahimian et al. 2015). Unlike conventional structures, OWTs constitute a large mass as rotor-nacelle-assembly (RNA) that result in activation and distribution of modal masses among various rotational and translation modes. Moreover, there remains a gap in the literature, regarding the suitability of an IM in describing a demand parameter for OWT-related performance limit states.

Therefore, the objective of this study is to evaluate the efficiency of S_a to represent seismic response of OWTs at three limit states. (i) Serviceability limit state (SLS) corresponds to deformation exceedance at tower top; (ii) Ultimate limit state (ULS) monitors the collapse by von Mises and/or buckling stresses; (iii) Initiation of emergency shutdown (ES) protocol for rotor operation due to excessive nacelle acceleration. Moreover, the seismic vulnerability of OWTs to pulse and non-pulse ground motions is assessed through non-linear dynamic analyses (NDA). A total of 80 pulse and 80 non-pulse records are selected. Each record contains two horizontal and one vertical component, leading to a sum of 480 accelerograms to perform NDA. The results are interpreted through a regression based nonlinear dynamic procedure referred to as the Cloud Analysis Method. The cloud method serves as an efficient tool to quantify the efficiency and relative sufficiency of a given IM (Ebrahimian et al. 2015).

2. STRUCTURAL MODEL

The standard specifications of the "NREL offshore 5MW baseline wind turbine", hereinafter referred to as 5MW, are adopted (Jonkman et al. 2009). The 5MW OWT is supported on a monopile foundation, designed by Stuttgart institute of Wind Energy (SWE), embedded 36m deep in an elastic homogenous soil stratum; unit weight γ_s and internal friction angle φ' shown in Figure 1.

The numerical model is developed using the open-source earthquake simulation package, i.e. OpenSees. The main tower, transition piece and monopile is modelled using non-linear displacement-based beam-column elements. Hollow circular fiber sections are adopted for non-prismatic main tower and prismatic transition piece and monopile. The monopile is modelled as beam on non-linear Winkler foundation (BNWF). The soil-pile interaction is considered through

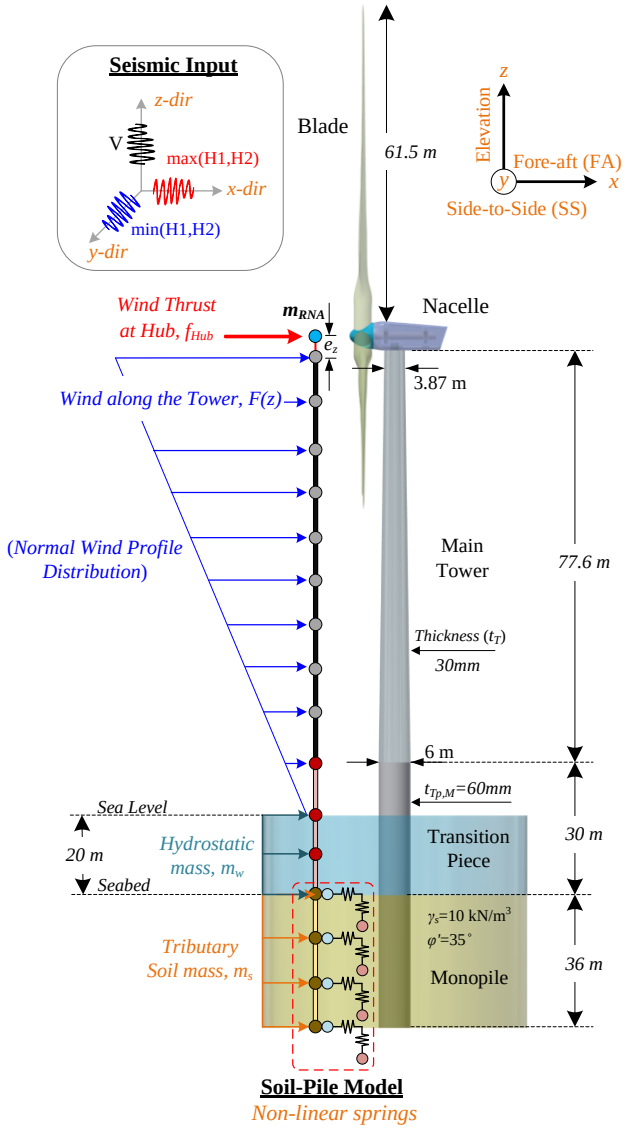

Figure 1: Schematic representation of the OWT, including soil-pile model, static inertial and dynamic loads.

API (2007) based non-linear p-y, t-z, and Q-z springs, which simulate lateral soil resistance, mechanical soil behavior along pile shaft, and its tip, respectively. Given insufficient geotechnical details, site amplification effects are currently unaccountable, thus, seismic motions are uniform along the monopile spring supports. Figure 2 shows first four fore-aft (FA) tower bending modes of the 5MW OWT, for brevity. The mass participation is uniformly distributed among higher modes and it require 18 modes to achieve over 90% mass activation in lateral and 80% in vertical direction.

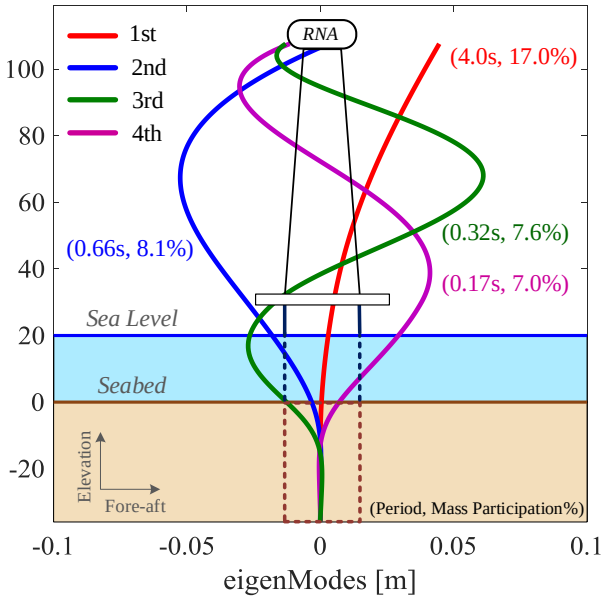

Figure 2: Mode shapes, periods and mass participation

2.1. Load Cases

Apart from self-weight applied as nodal masses, this study considers (i) rotary inertia of blades at the hub, located e_z=1.9626 m above the tower top; (ii) wind load along the tower and the wind thrust force acting at the hub; (iii) hydrostatic effect of the water mass on the submerged transition piece; (iv) tributary soil mass effect inside and outside the monopile; (v) earthquake load as acceleration time histories. Figure 1 shows schematic representation of 5MW OWT model, including its geometry, axes, wind, water and seismic load definition.

2.1.1. Wind loads

Normal wind profile (NWP) model is adopted to estimate the variation of mean wind speed along the tower height, $V(z)$, (IEC 61400-3 2009). It is then applied as static concentrated forces $F(z)$ at tower nodes, as follows;

$$V(z) = V_{Hub} \cdot \left({}^{z}/_{h_{Hub}}\right)^{0.2} \quad (1)$$

$$F(z) = 0.5 \cdot \rho_a \cdot V(z)^2 \cdot A(z) \quad (2)$$

where, V_{Hub} is the reference wind speed i.e., 15 m/s, acting at the hub; h_{Hub} is turbine's hub height above sea level; ρ_a is air density (1.25 kg/m^3); $A(z)$ is tributary area of the elements.

The effect of thrust forces at hub f_{Hub} is calculated, considering thrust coefficient C_T and rotor swept area (Arany et al. 2017).

$$f_{Hub} = 0.5 \cdot \rho_a \cdot V_{Hub}^2 \cdot (\pi \cdot R_T) \cdot C_T \quad (3)$$

$$C_T = 3.5 \cdot V_r \cdot (2 \cdot V_r + 3.5)/V_{Hub}^3 \quad (4)$$

where, R_T and V_r is the rotor radius and rated wind speed, respectively.

2.1.2. Hydrostatic and Tributary Soil Mass

Assuming stationary wave conditions, the hydraulic mass is added to submerged portion of the transition piece. This mass is assumed as 80% of the transition piece mass.

The effect of the soil mass inside and outside the hollow monopile is incorporated into the structural mass of the monopile. It is done by assuming a tributary area equivalent to pile dimension both inside and around it.

2.1.3. Record Selection and Seismic Input

The strong ground motions databases like NGA, K-NET, KiK-net and SK-net are utilized to select crustal records in the magnitude (M) range 6.0 to 8.0 and, rupture distance (R) up to 100km. A total of 160 crustal records constituting of 480-time histories are used for NDA. As shown in Figure 1, seismic input is organized to apply stronger horizontal component in the FA(x) direction parallel to wind loads whereas the weaker horizontal component is applied in the SS(y) direction. This is decided based on the higher

PGA value among the corresponding acceleration time-histories.

The selected records are further classified into three bins as follows;

(a) *Bin I*: 80 records, classified as pulse-like based on a seismic energy-based algorithm to detect strong velocity pulses inherent in near-fault ground motions (Chang et al. 2016).
(b) *Bin II*: 40 records, non-pulse with PGV greater than 30 cm/s.
(c) *Bin III*: 40 records, non-pulse with PGV less than 30 cm/s.

The notable PGV-based differentiation between non-pulse records in *Bin II* and *III* is to establish a viable comparison with pulse-like records. As the pulse extraction method adopted herein, uses a PGV threshold of 30cm/s, for more details, see (Chang et al. 2016).

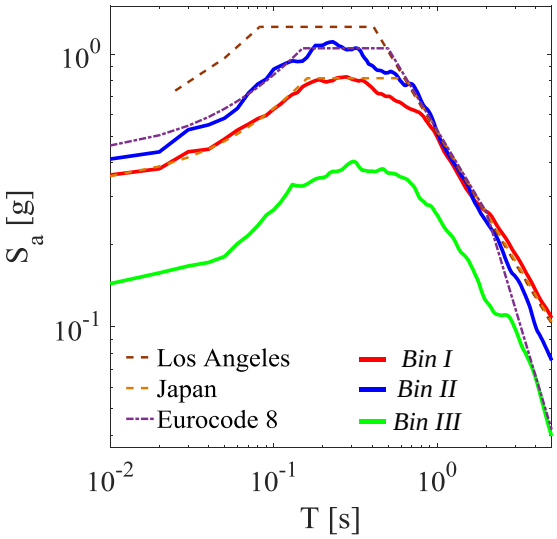

Figure 3: Geometric mean of horizontal response spectra with uniform hazard spectra at various seismic locations; in logarithmic scale

Figure 3 shows mean response spectra of three record bins and their compatibility with design/uniform hazard spectrum (UHS) of three active seismic locations for Soil Class B and 10% probability in 50 years. At long periods above 1.0s, *Bin I* and *II* records are coherent with all target spectra. However, at shorter periods *Bin I* and *II* is more compatible with Japanese and Eurocode 8 design spectrum, respectively. In case of *Bin III*, overall trend is weaker expect at periods above 2.5s, which agrees with Los Angeles UHS.

3. ANALYSES, LIMIT STATES AND DEMAND PARAMETERS

3.1. Cloud Analysis

Cloud analysis refers to a regression-based probabilistic model to represent a decision variable and/or engineering demand parameter for a given IM. The decision variable is taken to be the critical demand over capacity ratio for a given limit state, Y_{LS}, obtained through non-linear time history analyses to fit against the chosen IM. First-mode spectral acceleration $S_a(T_1)$ herein chosen to be the candidate IM. Therefore, for a suite of N records, $Y_{LS} = \{Y_{LS,i}, i = 1{:}N\}$ and corresponding values of $S_a = \{S_{a,i}, i = 1{:}N\}$ are two datasets of cloud analysis, paired and graphically described as scattered plots for an *i*th ground motion record (Jalayer et al. 2017). The regression model describes the expected value E for natural logarithm of Y_{LS} given S_a and the associated variability $\beta_{Y_{LS}|S_a}$ in Eq. (5) & (6), respectively;

$$\mathrm{E}\left[\ln Y_{LS}|S_a\right] = \ln \eta_{Y_{LS}|S_a} = \ln a + b \ln S_a \qquad (5)$$

$$\beta_{Y_{LS}|S_a} = \sigma_{\ln Y_{LS}|S_a} = \sqrt{\sum_{i=1}^{N}\left(\ln Y_{LS,i} - \ln \eta_{Y_{LS,i}|S_{a,i}}\right)^2/(N-2)} \qquad (6)$$

where $\sigma_{\ln Y_{LS}|S_a}$ is the conditional standard deviation, equivalent to $\beta_{Y_{LS}|S_a}$ generally referred to as variability or dispersion. $\beta_{Y_{LS}|S_a}$ predicts the efficiency of a candidate IM quantitively. Its value in the range of 0.20 to 0.30 remarks credible efficiency of an IM (Mollaioli et al. 2013).

3.2. Limit States and Demand Parameters

The structural performance is quantified adhering to code provisions and recent literature on OWTs. Three limit states relating to serviceability (SLS), ultimate conditions (ULS) and emergency shutdown (ES) protocol are studied. The corresponding demands (*D*) and capacities (*C*) to

evaluate the performance variable Y_{LS} are summarized in Table 1.

Eq. (7) & (8) ensures strength and stability of steel shell structures and correspond to *Von-Mises Equivalent Design Stress* (σ_{eq}) and *Buckling Strength Check through Stress Limitation* criteria, respectively. σ and τ are meridional stress and planar shear stress; f_y is the yield strength = 355 MPa for S355 steel. For more details, refer to Annex D of (EN 1993-1-6 2007). To our knowledge, no explicit threshold is available on nacelle acceleration, exceeding which would initiate the emergency rotor shutdown (ES) protocol. Therefore, maximum nacelle

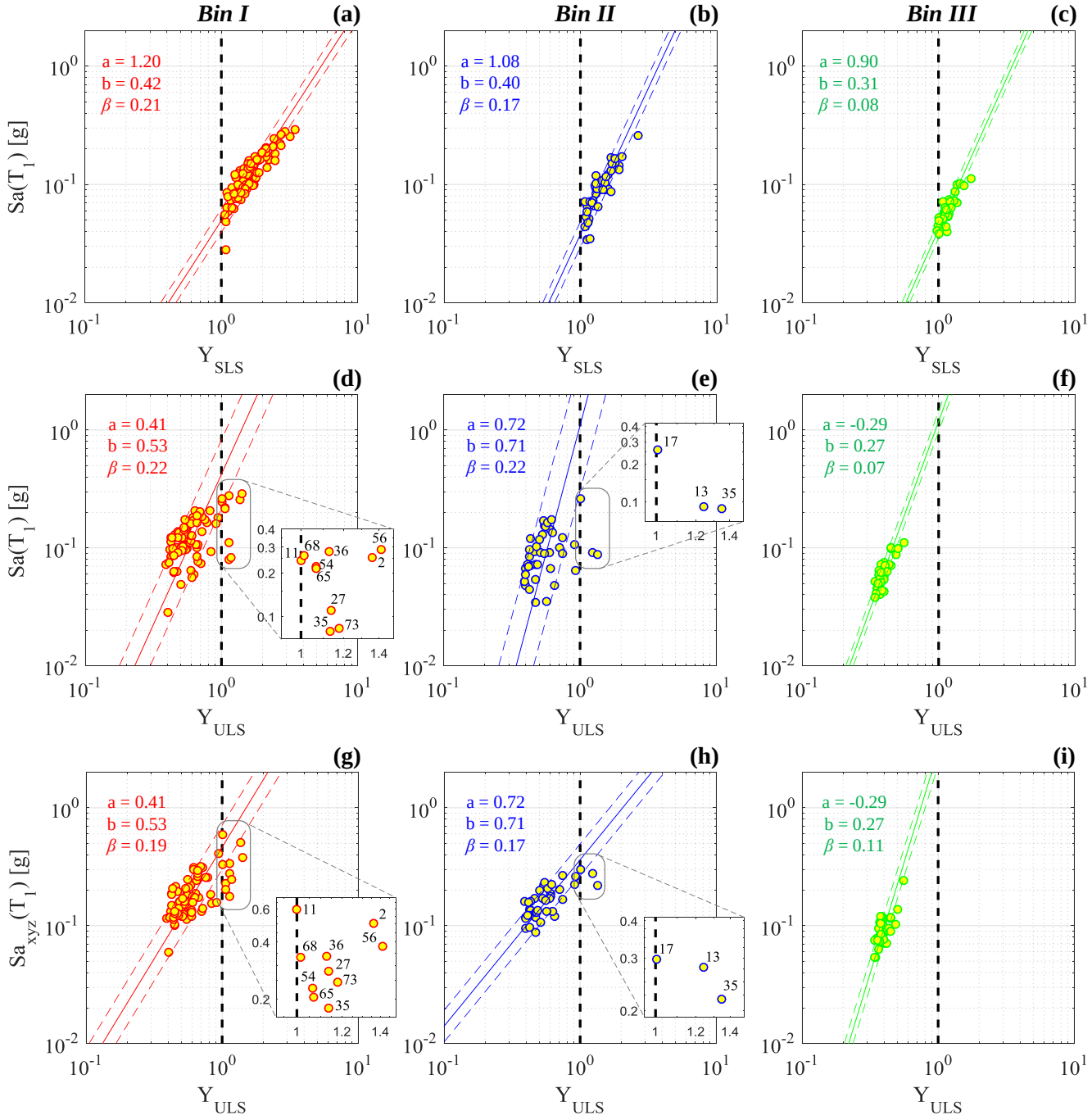

Figure 4: Cloud scatter plots of Y_{SLS} and Y_{ULS} given $S_a(T_1)$ for pulse (Bin I) and non-pulse (Bin II and III) records

acceleration described in Table 1 is taken as the capacity.

Table 1: Demand and capacity at a given LS.

Limit State	*D*	*C*	Reference
SLS	*Tower top Rotation*	*±0.5°*	(DNV GL 2014)
ULS	*Stress Ratio; max of Eq. (7) & (8)*	*1*	(EN 1993-1-6 2007)
ES	*Nacelle Acceleration*	*1 m/s²*	(Katsanos et al. 2017)

$$Y_{ULS} = \frac{D}{C} = \frac{\sigma_{eq}}{f_y} = \sqrt{\sigma^2 + 3.\tau^2}/f_y \leq 1 \quad (7)$$

$$Y_{ULS} = \left(\frac{\sigma}{\sigma_{x,Rd}}\right)^{k_x} + \left(\frac{\tau}{\tau_{x\theta,Rd}}\right)^{k_\tau} \leq 1 \quad (8)$$

4. RESULTS

The scatter plots for data pairs of performance variable Y_{LS} and S_a for three bins of records and the associated logarithmic standard deviation of residuals, $\beta_{Y_{LS}|S_a}$, obtained from the cloud regression model are presented and discussed in this section. The solid line represents the estimated regression; dashed lines show one-logarithmic standard deviation; *a* is the ordinate intercept and *b* is the slope of the regression line.

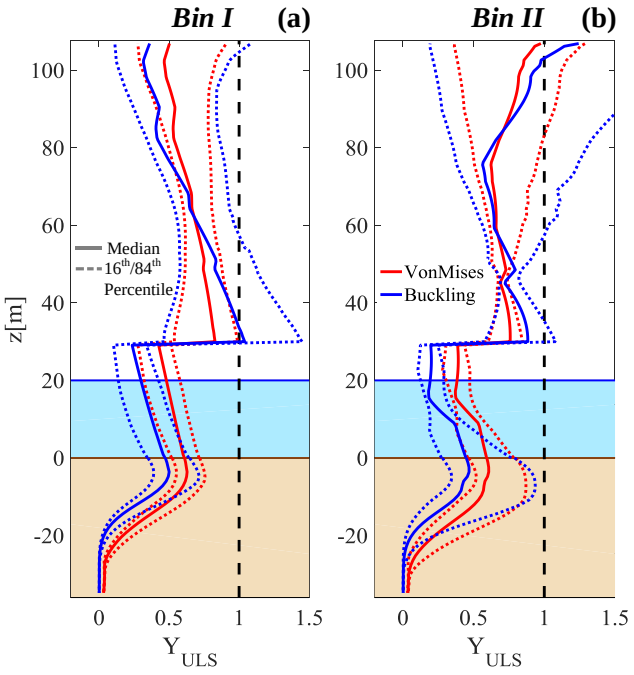

Figure 5: Stress variation for records exceeding Y_{ULS}

4.1.1. *Serviceability and Ultimate Limit State*

Figure 4 plots the cloud scatter of Y_{SLS} and Y_{ULS} versus $S_a(T_1) = \sqrt{S_{a,x}(T_1) \cdot S_{a,y}(T_1)}$ for pulse and non-pulse records of *Bin I* and *II*, *III*, respectively. At SLS, low record-to-record variability is achieved, and all records have shown great tendency to exceed Y_{SLS}. Notably in Figure 4(a-c), for lower $S_a(T_1)$ values at long natural period of vibration (4s), all records regardless of their classification exceeded the performance limit. This may be attributed to low soil density and code provisions which suggest ±0.5° as allowable rotation for the pile head, however, there are no explicit guidelines for tower of varying slenderness, height, etc. Therefore, the applicability of these outcomes depends on the current state of practice.

Figure 4(d-f) show record-to-record variability of Y_{ULS} to corresponding $S_a(T_1)$ values. The 5MW OWT model is sensitive to *Bin I* and *II* records with considerable number of records causing the collapse condition. In view of dispersion, an adequate estimate is achieved, however, some records exhibit visually high dispersion and exceeded Y_{ULS} for relatively low $S_a(T_1)$ values. This observation is highlighted in the zoomed portion of Figure 4(d & e). Therefore, to understand the cause of such scatter, $S_a(T_1)$ is modified to include $S_{a,z}(T_1)$; such that $S_{a,xyz}(T_1) = \left(S_{a,x}(T_1) \cdot S_{a,y}(T_1) \cdot S_{a,z}(T_1)\right)^{1/3}$. As shown in Figure 4(g & h), the inclusion of vertical component increased $S_{a,xyz}(T_1)$ values for records showing low $S_a(T_1)$ values in parts (d & e) of the figure. This improves $\beta_{Y_{ULS}|S_a}$ from 0.22 to 0.19 for *Bin I* records and 0.22 to 0.17 for *Bin II* records. It also signifies the importance of considering records with strong vertical component in the collapse assessment of OWTs. As not only, it leads to improved cloud dispersion, but also indicates the possible failure mechanism, i.e. buckling. Figure 5 shows the contribution and distribution of vonMises and buckling stresses

along the tower, and possible failure locations. The median lines indicate failure by buckling at base and top of the main tower because of *Bin I* and *II* records, respectively. The stress concentration at tower base is due to differing transition piece thickness, shown in Figure 1: Schematic representation of the OWT, including soil-pile model, static inertial and dynamic loads.. Notable records exceeding Y_{ULS} contain strong vertical component, inducing meridional compressive stresses, in turn, leading to tower buckling.

4.1.2. Emergency Shutdown

Spectral acceleration at nacelle/tower top $S_{a(Top)}$ is assessed for higher mode response, shown in Figure 6. Given first four modes dominating the response at nacelle location, $S_a(T_1)$ is modified to include their effect in describing Y_{ES} . The modified IM is taken as geometric mean of first four FA and SA modes, i.e., n = 8 in Eq.

$$AvgS_a(T_1, \dots, T_n) = \left(\prod_{i=1}^{n} S_a(T_i)\right)^{1/n} \quad (9)$$

The corresponding scatter plots are shown in Figure 7. The modified IM leads to a good fit and low variability for three record bins. Notable number of records tends to initiate emergency shutdown for rotor operation, particularly for *Bin I* and *II*. As expected, turbine is insensitive to *Bin III* records due to low spectral accelerations at the higher modes and weaker PGV content, i.e., less than 30 cm/s.

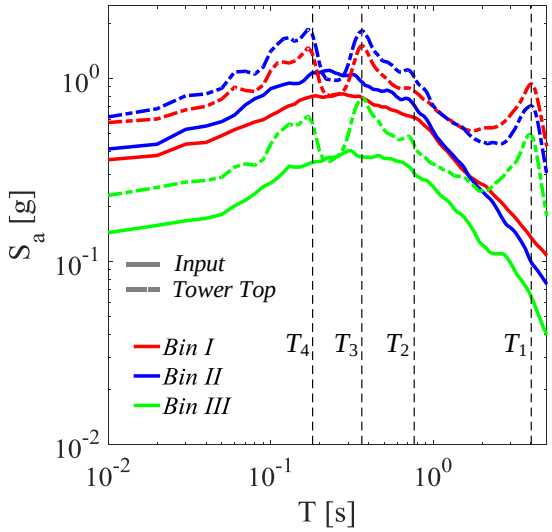

Figure 6: Response spectra of selected records and tower top acceleration.

5. CONCLUSIONS

This study evaluates the efficiency of spectral acceleration to describe structural performance variable of offshore wind turbines (OWT) at three prescribed limit states through cloud-based approach. The sensitivity of a 5MW OWT to pulse and non-pulse crustal records is evaluated. The conclusions drawn from this study are as follows;

1) $S_a(T_1)$ is an efficient intensity measure (IM) for response prediction of OWTs at serviceability limit state (SLS). The

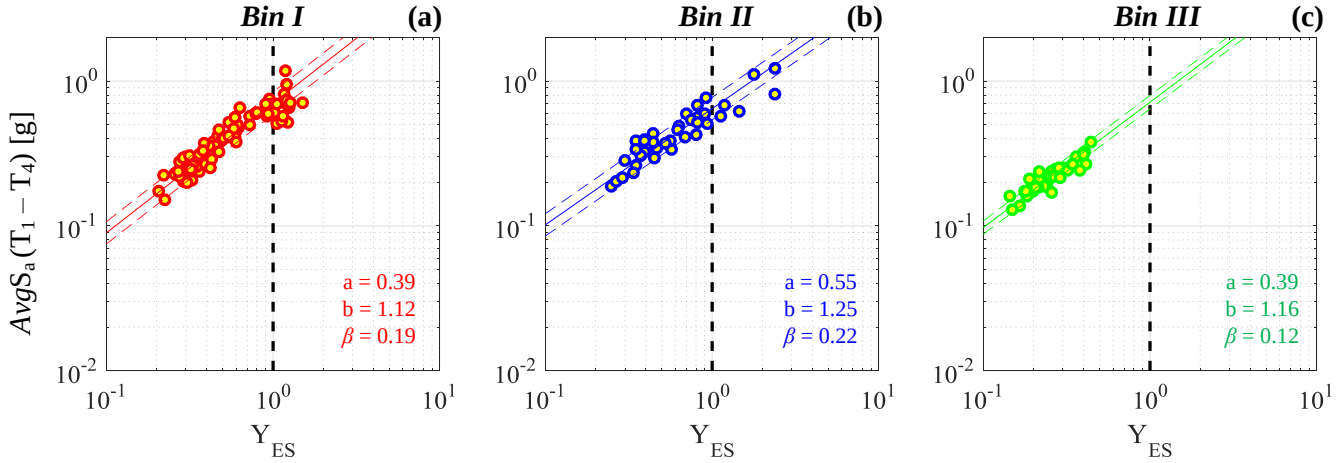

Figure 7: Cloud analysis results of Y_{ES} given $AvgS_a(T_1 - T_4)$

dispersion may increase based on PGV content and presence of pulse in the records.

2) Similarly, at ultimate limit state (ULS), $S_a(T_1)$ describes response variability with acceptable accuracy. However, the dispersion can be further improved by considering the effects of strong vertical accelerations, if present in the selected suite of records for nonlinear dynamic analyses.
3) For emergency shutdown (ES), average spectral acceleration ($AvgS_a$) is a better IM, due to activation of higher modes.
4) In view of seismic vulnerability to pulse and non-pulse records, OWTs can undergo excessive deformations regardless of earthquake types, considered herein. At ULS and ES, pulse-like and non-pulse records with *PGV*>30cm/s dominant the response. The presence of strong vertical accelerations may cause tower buckling failure at its base and top, which should be thoroughly addressed in the future studies. Moreover, nacelle accelerations can amplify to trigger the operational stoppage of the rotor. A detailed incremental dynamic analysis must be conducted to obtain more reliable insight on the collapse conditions.

6. REFERENCES

Alati, N., Failla, G., and Arena, F. (2015). "Seismic analysis of offshore wind turbines on bottom-fixed support structures." *Phil. Trans. R. Soc. A*, The Royal Society, 373(2035), 20140086.

API. (2007). "Recommended Practice for Planning , Designing and Constructing Fixed Offshore Platforms — Working Stress Design." *Api Recommended Practice*, 24–WSD(December 2000), 242.

Arany, L., Bhattacharya, S., Macdonald, J., and Hogan, S. J. (2017). "Design of monopiles for offshore wind turbines in 10 steps." *Soil Dynamics and Earthquake Engineering*, Elsevier, 92(September 2016), 126–152.

Chang, Z., Sun, X., Zhai, C., Zhao, J. X., and Xie, L. (2016). "An improved energy-based approach for selecting pulse-like ground motions." *Earthquake Engineering & Structural Dynamics*, Wiley Online Library, 45(14), 2405–2411.

DNV GL. (2014). *Design of Offshore Wind Turbine Structures (DNV-OS-J101). Det Norske Veritas AS, Oslo*.

Ebrahimian, H., Jalayer, F., Lucchini, A., Mollaioli, F., and Manfredi, G. (2015). "Preliminary ranking of alternative scalar and vector intensity measures of ground shaking." *Bulletin of Earthquake Engineering*, Springer Netherlands, 13(10), 2805–2840.

EN 1993-1-6. (2007). "Eurocode 3: Design of Steel Structures-Part 1-6: Strength and Stability of Shell Structures." Comite´ Europe´en de Normalisation, Brussels, Belgium.

IEC 61400-3. (2009). *Wind Turbines-Part 3: Design Requirements for Offshore Wind Turbines*. *Tech. Rep.*, International Electrotechnical Commission Geneva, Switzerland.

Jalayer, F., Ebrahimian, H., Miano, A., Manfredi, G., and Sezen, H. (2017). "Analytical fragility assessment using unscaled ground motion records." *Earthquake Engineering and Structural Dynamics*, 46(15), 2639–2663.

Jonkman, J., Butterfield, S., Musial, W., and Scott, G. (2009). "Definition of a 5-MW Reference Wind Turbine for Offshore System Development." (February).

Kalkan, E., and Kunnath, S. K. (2006). "Effects of fling step and forward directivity on seismic response of buildings." *Earthquake spectra*, 22(2), 367–390.

Katsanos, E. I., Sanz, A. A., Georgakis, C. T., and Thöns, S. (2017). "Multi-hazard response analysis of a 5MW offshore wind turbine." *Procedia engineering*, Elsevier, 199, 3206–3211.

Kim, D. H., Lee, S. G., and Lee, I. K. (2014). "Seismic fragility analysis of 5MW offshore wind turbine." *Renewable Energy*, Elsevier Ltd, 65, 250–256.

Mollaioli, F., Lucchini, A., Cheng, Y., and Monti, G. (2013). "Intensity measures for the seismic response prediction of base-isolated buildings." *Bulletin of Earthquake Engineering*, 11(5), 1841–1866.

De Risi, R., Bhattacharya, S., and Goda, K. (2018). "Seismic performance assessment of monopile-supported offshore wind turbines using unscaled natural earthquake records." *Soil Dynamics and Earthquake Engineering*, Elsevier, 109, 154–172.